Biophysical Journal, Volume *117*

Supplemental Information

A General Workflow for Characterization of Nernstian Dyes and Their Effects on Bacterial Physiology

Leonardo Mancini, Guillaume Terradot, Tian Tian, YingYing Pu, Yingxing Li, Chien-Jung Lo, Fan Bai, and Teuta Pilizota

A general work-flow for the characterization of Nernstian dye candidates and their effects on bacterial physiology

L Mancini[1], G Terradot[1,*], T Tian[2,*], Y Pu[2], Y Li[2], CJ Lo[3], F Bai[2], and T Pilizota[1,+]

[*]**these authors contributed equally to this work**
[+]**Corresponding author:teuta.pilizota@ed.ac.uk**

SUPPLEMENTARY FIGURES

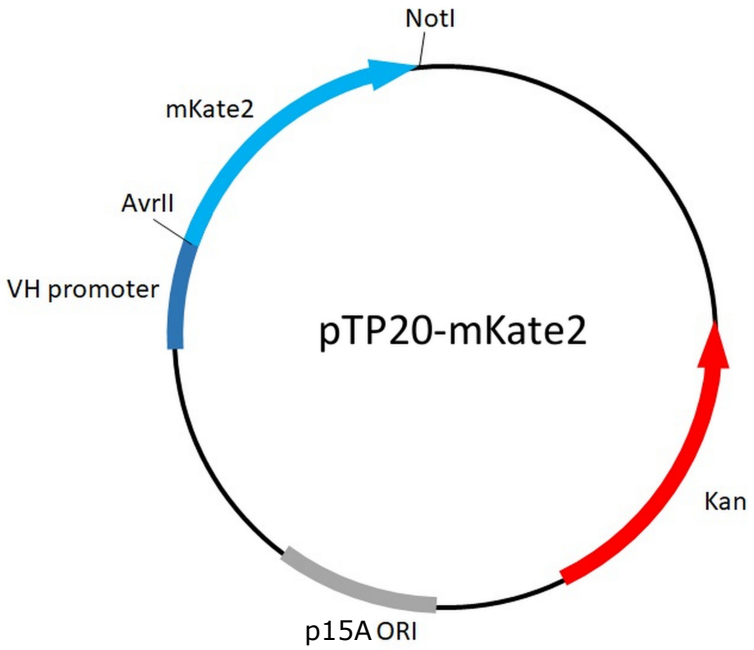

Supplementary figure 1. Plasmid map of pTP20-mKate2 showing the insertion site of mCherry-mKate2 hybrid (mKate2 for brevity) [1]. The constitutive cytochrome oxidase promoter from *Vibrio Harveyi* [2], the origin of replication and the Kanamycin resistance cassette are indicated.

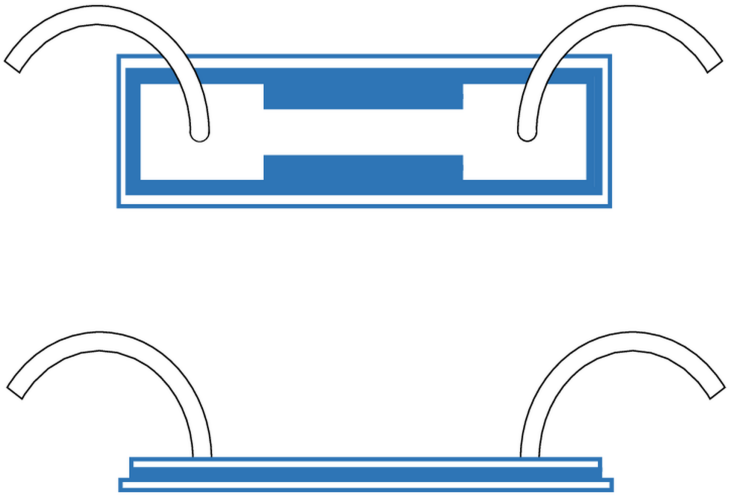

Supplementary figure 2. Schematic of our flow-cell. Microscope slide and coverslip are held together by custom cut Gene Frames (Thermo Fisher Scientific, UK). To exchange liquids, we drill two holes on the microscope slide and attach tubing using epoxy glue on the outside of the slide [3].

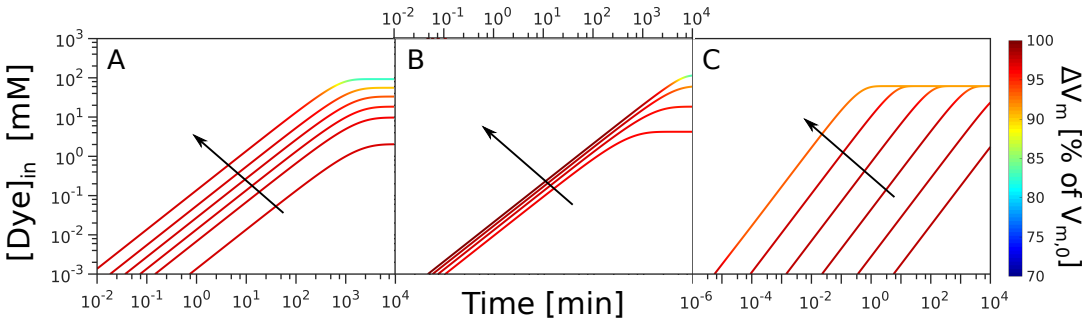

Supplementary figure 3. Dynamics of the dye loading assuming GHK rate law for leakage (Eq. (14)), where we assumed Eyring rate (law Eq. (13)) in Fig. 2 of the main text. (A) Intracellular Dye concentration as a function of time, for extracellular dye concentrations 10, 50, 100, 200, 400 and 1000 μM. The arrow indicated increasing $[Dye]_{out}$, and $V_{m,0} = -140$ mV, $Y_i = 150$ mM, $\Delta G_E = -210$ mV. (B) Intracellular dye concentration as a function of time for different $V_{m,0}$: -220, -180, -140 and -100 mV. The arrow indicates increasing absolute value of the $V_{m,0}$, and $[Dye]_{out} = 100$ μM, $Y_i = 150$ mM and $\Delta G_E = -210$ mV. (C) Intracellular dye concentration as a function of time for different apparent permeabilities of the membrane (with respect to the dye): 10^{-12}, $10^{-10.8}$, $10^{-9.6}$, $10^{-8.4}$, $10^{-7.2}$, 10^{-6} m/s. The arrow indicates increasing permeability, and $V_{m,0} = -180$ mV, $Y_i = 150$ mM, $\Delta G_E = -210$ mV and $[Dye]_{out} = 100$ μM.

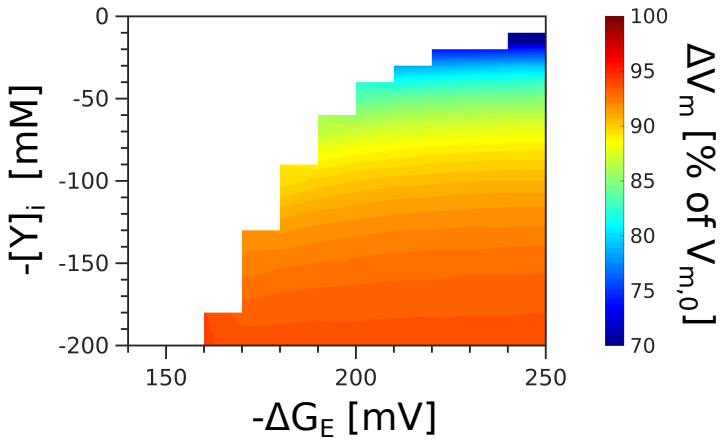

Supplementary figure 4. ΔV_m depends on the free energy available for transport of $[C^+]$ as well as on the contribution of charged impermeable species ($[Y_i]$), even for the same value of $V_{m,0}$. $[Dye]_{out} = 100\ \mu$M. $V_{m,0} = -180$ mV. Colour scale on the right gives ΔV_m values.

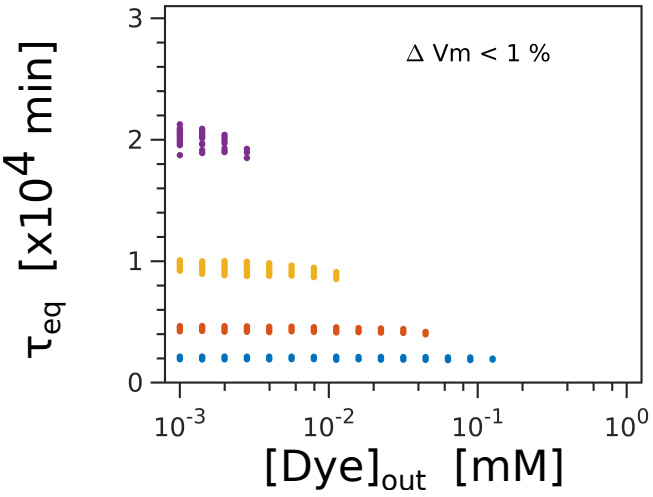

Supplementary figure 5. Equilibration time, τ_{eq}, as a function of $[Dye]_{out}$ for different $V_{m,0}$ values. The permeability of the dye was set to $P_{Dye} = 10^{-10}$ m/s. Purple, yellow, red and blue are $V_{m,0}$ of -220, -180, -140 and -100 mV (± 5 mV), respectively. For each value of $[Dye]_{out}$ we plot all the values of τ_{eq} that yield the desired $V_{m,0} \pm 5$ mV, where $\{[Y]_{in}, \rho, \Delta G_E\}$ were varied in the range specified in Table 4. The simulations that change $V_{m,0}$ by less than 1% mV are plotted, showing that when $\Delta V_m \sim 0$, τ_{eq} is a function of $V_{m,0}$ only.

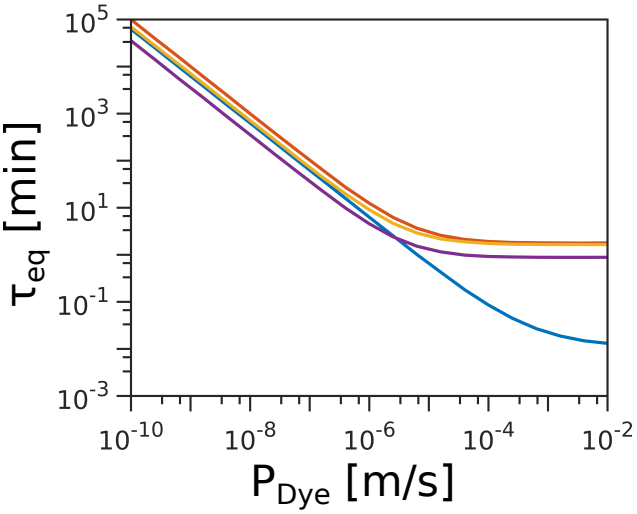

Supplementary figure 6. Equilibration time, τ_{eq}, as a function of the dye permeability. The following were set: $[Y]_i = 150$ mM, $\Delta G_E = -210$ mV, $[Dye]_{in} = 100$ μM. The blue, red, yellow and purple lines are for $V_{m,0}$ of -220, -180, -140 and -100 mV, respectively. For each of them, ΔV_m is permeability invariant and takes the respective values of 83%, 93%, 96% and 97%.

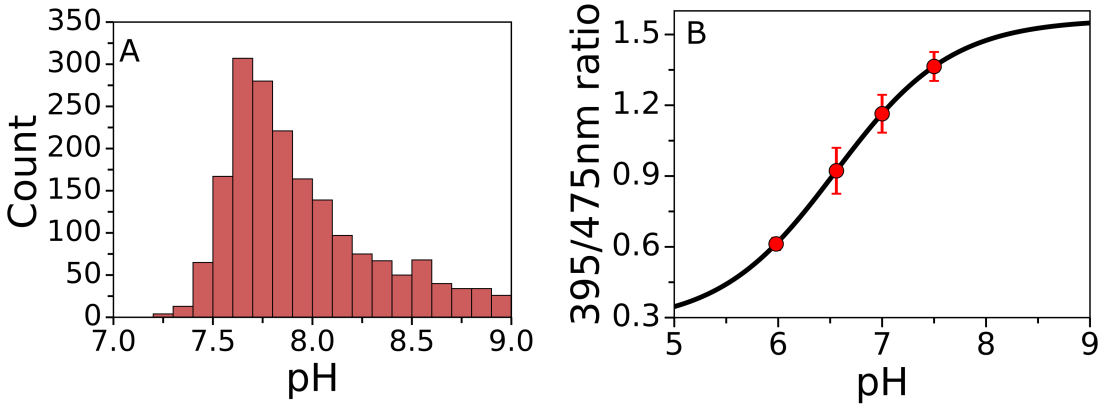

Supplementary figure 7. Intracellular pH measurements. (A) Using chromosomally expressed pHluorin [3, 4] we measure intracellular pH in 2346 individual cells. The median value of the distribution is 7.86. (B) *In vivo* pHluorin calibration curve where the cells were exposed to 40 mM potassium benzoate and 40mM methylamine hydrochloride in order to collapse internal pH [4]. Data points are an average of $\sim$400 cells and error bars give the standard deviation.

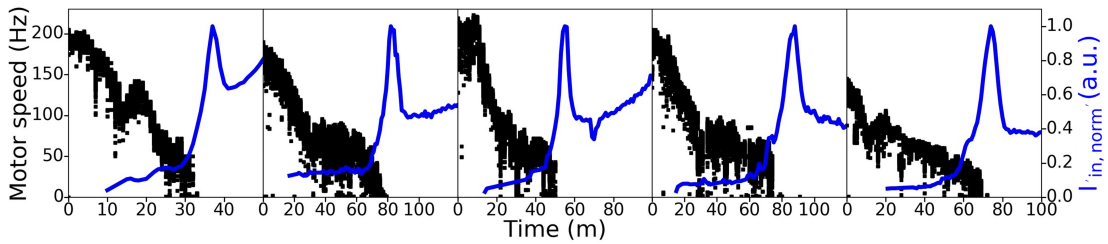

Supplementary figure 8. Individual motor traces (black) that were averaged in Fig. 5A. ThT intensity traces are given in blue, and imaging and exposure setting are as specified in *Material and Methods*.

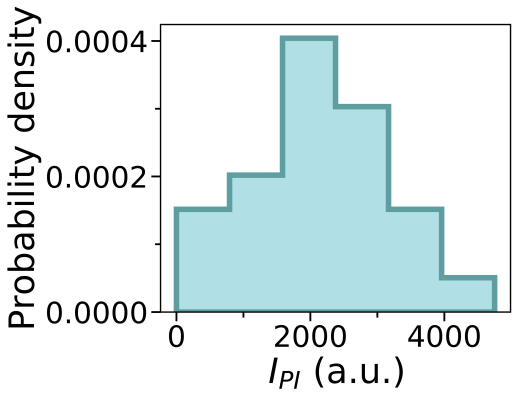

Supplementary figure 9. Probability density function of the final intensity values of propidium iodide from Fig. 5B ($I(t_f)$ with t_f = 185 min). Cell count is 25 from 3 different experiments.

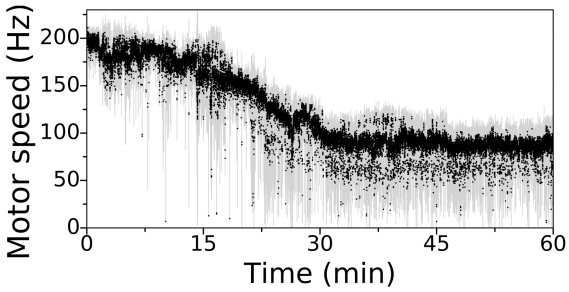

Supplementary figure 10. Light-induced damage quantified by measuring PMF loss via bacterial flagellar motor speed, over the length of an hour. The experiment was carried out as in Fig. 5A, but ThT was not added to the MM9 + glucose media, which was continuously supplied through out the experiment with a flow rate of 50 μl/min. Black shows the average of three individual motor speed recordings, each on a different cell, and grey area shows the standard deviation.

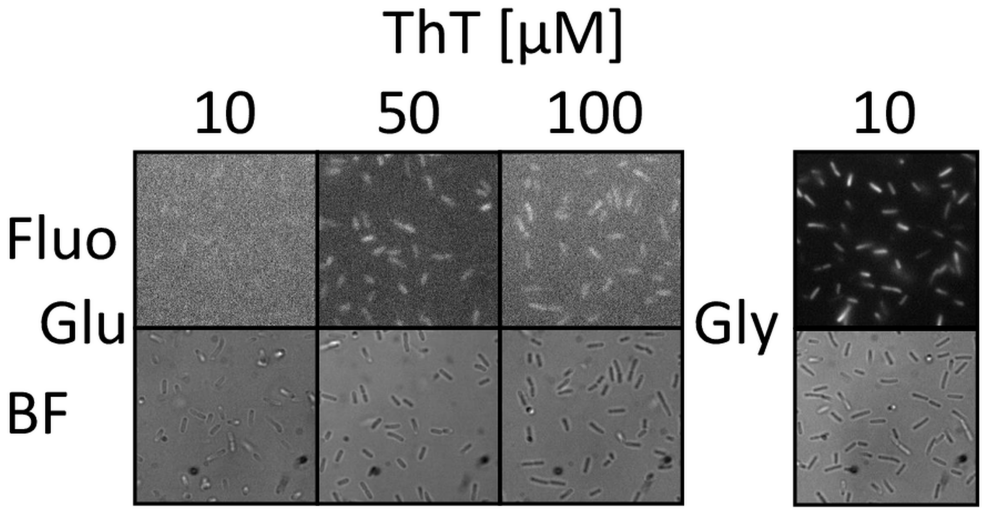

Supplementary figure 11. Cells grown in the plate reader (Fig 3A, B and C) in the presence of ThT were imaged, in order to estimate the extent of dye equilibration. "Fluo" abbreviation indicates fluorescence intensity and "BF", the brightfield image. Imaging conditions for ThT are the same as those used throughout the paper (Fig.3D E, 4A, 5A, B, C D). Cells were imaged after 7 h of growth in the plate reader (OD= 0.5- 0.6 when grown on glucose and 0.4 on glycerol) when 10 and 50 μM ThT was present, and after 8.5 h (OD 0.7 when grown on glucose) for the 100 μM ThT case.

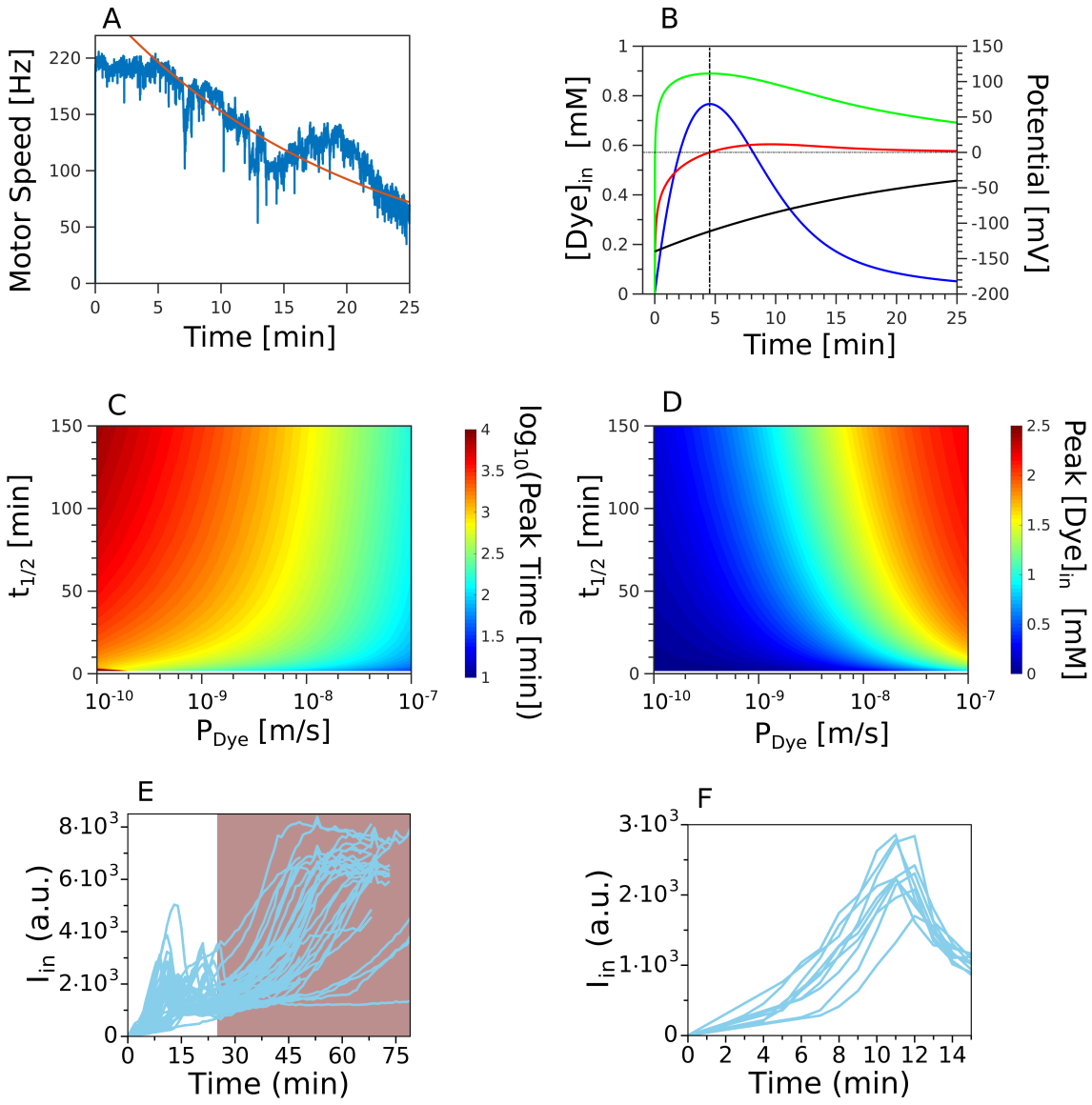

Supplementary figure 12. (A) Exponential decay of V_m during ThT loading leads to an intensity peak. Exponential fit (in red and starting from the time we observe the decay) to the first motor speed trace shown in Fig. SI5. The half-time of the decay is $t_{1/2} = 16.4$ min, which we use as the decay time of V_m. (B) Dye equilibration profile for the case of exponentially decaying V_m (black) is plotted in blue. The permeability of the dye was set to $P_{Dye} = 10^{-8}$ m/s, $[Dye]_{out} = 10^{-2}$ mM, and $V_{m,0} = -140$ mV. Green line depicts the contribution of the concentration gradient to the dye electrochemical potential $\ln([Dye]_{in}/[Dye]_{out})$ and red line the electrochemical potential of the dye. (C) Peak time (in log scale) and (D) peak intracellular dye concentration as a function of $t_{1/2}$ and the dye permeability. For both (C) and (D) we assumed $V_{m,0} = -140$ mV. (E) The model is relevant for the part of the equilibration profile that is driven by V_m. Subsequent increase in ThT intensity (shaded in red) does not obey Nernstian equation, because V_m is zero (Fig. 5A) and cell membrane is compromised (Fig. 5B). The traces are reproduced from Fig. 3D. (F) 10 example traces from Fig. 3D showing the portion of the equilibration curve described by our model.

SUPPLEMENTARY VIDEOS

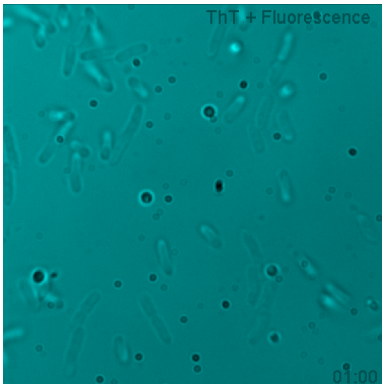

Supplementary video 1. *E. coli* growing in LB medium in our flow cell before addition of the ThT dye (images shown in gray-scale). In yellow we colour the frames that correspond to addition of the dye but without epifluorescence imaging. While the dye is present in the medium, it does not enter the cytoplasm, and thus the cells continue to grow. We colour in cyan the frames where both the ThT and epifluorescence imaging is happening at the same time. ThT now enters the cytoplasm and cells stop growing. The brightfield images correspond to one of the experiments presented in Fig. 5E.

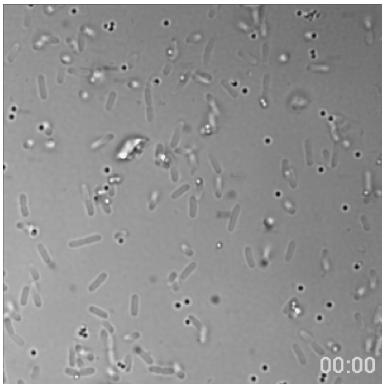

Supplementary video 2. Growth of *E. coli* in our flow cell, in MM9 + glucose medium, in the presence of epifluorescence illumination. The brightfield images are from one of the experiments in Fig. SI10. Cells grow in our flow cell when epifluorescence imaging is turned on.

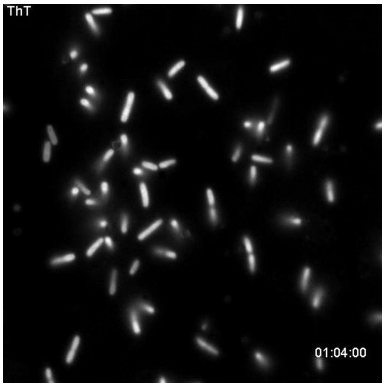

Supplementary video 3. Equilibration of ThT in LB. Dynamics of ThT equilibration in a flow slide in LB medium from the experiments in Fig. 3D. Images are taken every minute.

Supplementary video 4. Characteristic single cell volume change and cytoplasmic marker loss during ThT equilibration. Dynamics of cytoplasmic mKate2 fluorescent signal (right) during ThT equilibration (left) from the experiment in Fig. 5 C. Images are taken every minute.

SUPPLEMENTARY TABLES

Plasmid	Fragment	Primers
pTP20-mKate2	pWR20 backbone [2]	5' AAAGCGGCCGCGGTGATTGATTGAGCAAG 3' 5' AAACCTAGGATGTATATCTCCTTAACTAGGT 3'
pTP20-mKate2	mCherry-mKate2 hybrid [1]	5' AATGCGGCCGCTTATCTGTGCCCCAGTTT 3' 5' ATACCTAGGATGGTTAGTAAAGGAGAAGAA 3'

Table 1. Plasmids and primers used in this work.

Strain	Origin	Figure
MG1655		3, 4A, 5B, 5E, 5D and SI 2, 9
MG1655-*pTP20-mKate2*	This work	5C
EK01	[3]	5A and SI 4,5,7
EK07	[3]	SI 10
BW25113 Δ*tolC* pTP20-mKate2	This work	4A, 4B

Table 2. List of *E. coli* strains used in this work.

Name	Symbol	Value	Units	Reference
Faraday constant	F	96485	C/mol	
Gas constant	R	8.31	J/mol/K	
Temperature	T	298	K	
Avogadro Number	N_A	6.02×10^{23}	mol^{-1}	
Cell length	l_{cell}	2.95×10^{-6}	m	[5]
Cell width	w_{cell}	1.07×10^{-6}	m	[5]
Cell surface	S_{cell}	9.91×10^{-12}	m^2	Eq. SI(3)
Cell volume	V_{cell}	2.33×10^{-18}	m^3	Eq. SI(4)
Membrane Specific Capacitance	C_m	6.5×10^{-3}	$\mathrm{F/m}^2$	[6]
Total Membrane Capacitance	C	6.45×10^{-14}	F	Eq. SI(2)
Total Extracellular ionic concentration	Π_e	200	$\mathrm{mol/m}^3$	
Membrane Permeability to C^+	P_{C^+}	1.8×10^{-9}	m/s	[7] (K^+)
Membrane Permeability to A^-	P_{A^-}	1.4×10^{-10}	m/s	[7] (Cl^-)

Table 3. Parameters used for the simulations. The cell length and width in MM9+glucose were obtained from our fluorescence microscopy measurements and are consistent with [5].

Sampled parameters	Range of values	Spacing	Number of values
ΔG_E	$-250\mathrm{mV} \leq \Delta G_E/F \times 10^{-3} \leq -50\mathrm{mV}$	Linear	21
$[Y]_{in}$	$0 \leq [Y]_{in} \leq 200$ Moles/meter^3	Linear	21
ρ	$10^{-4} \leq \rho \leq 10^5$	$\log_{10}$	1000

Table 4. Value of parameters used when solving Eqs. SI 20 and 21 to obtain $V_{m,0}$.

SUPPLEMENTARY TEXT

Supplementary methods

Intracellular pH estimation.

To estimate the intracellular pH we used *EK07* cells grown to OD 0.8 in TB at 30°C and transferred to MM9 + glucose media, as for the experiments in Fig. 5A and as in [8]. Imaging was carried out in a flow-cell with a 50 ms exposure time and gain set to 300. Illumination at 395 nm and 470 nm was provided by a narrow spectrum UV LED and a Neutral White LED (Cairn Research Ltd, UK), respectively [3]. The filters used were ET470/40x and ET525/40m (Chroma Technology, USA) for the excitation at 470 nm and the emission of both [3]. The *in vivo* calibration curve of *EK07* cells expressing pHluorin was obtained by collapsing cytoplasmic pH using 40 mM potassium benzoate and 40 mM methylamine hydrochloride [9]. The mixture was added to MM9 + glucose media and the pH of the solution was adjusted to 5.98, 6.56, 7 or 7.5, respectively. The media at different pH were introduced into the flow-cell and imaging was carried out 5 min after [10]. Data was fitted to a sigmoid: $R395/475 = \frac{a_1 e^{k(pH-pH_0)} + a_2}{e^{k(pH-pH_0)} + 1}$ where a_1, a_2, k and pH_0 are fitting parameters as in [3] (a_1 = 1.56449665, a_2 = 0.27090295, k = 1.79203546 and pH_0 = 6.55202883).

Detailed description of the model

As mentioned in the main text we treat the *E. coli's* membrane as a parallel-plate capacitor and write the V_m as [11]:

$$V_m = F \cdot \frac{Q_{in}}{C} \tag{1}$$

where Q_{in} is the intracellular total charge (in mole) and C the membrane capacitance that depends on the membrane specific capacitance and the cell's surface area:

$$C = S_{cell} \cdot C_m \tag{2}$$

To calculate S_{cell} we assume the cell is a spherocylinder with 3:1 length to width ratio (determined from our microscopy images and consistent with [5]) and write as in [12]:

$$S_{cell} = \pi w_{cell} \cdot l_{cell} \tag{3}$$

$$V_{cell} = \pi \left(\frac{w_{cell}}{2}\right)^2 \left(l_{cell} - \frac{w_{cell}}{3}\right) \tag{4}$$

where l_{cell}, w_{cell} and V_{cell} are cell length, width and volume respectively.

Equation (3) in the main text lists the ionic species that contribute to Q_{in} and we assume electroneutrality in the extracellular space such that:

$$[C^+]_{out} - [A^-]_{out} + [Dye]_{out} = 0 \tag{5}$$

We keep the total ionic concentration in the extracellular medium, Π_e, fixed in the simulations:

$$[C^+]_{out} + [A^-]_{out} + [Dye]_{out} = \Pi_e \tag{6}$$

Consequently from SI Eqs. (5) and (6), the ionic composition of the medium only depends on the choice of $[Dye]_{out}$ and follows:

$$[C^+]_{out} = \frac{\Pi_e}{2} - [Dye]_{out} \tag{7}$$

$$[A^-]_{out} = \frac{\Pi_e}{2} \tag{8}$$

Separation of charges, and thus V_m, is governed by two type of reactions: leakage and active pumping, which means that the intracellular concentration of charged species we consider, changes in time as follows:

$$\frac{d[A^-]_{in}}{dt} = j_{L,A^-} \tag{9}$$

$$\frac{d[Dye]_{in}}{dt} = j_{L,Dye} \tag{10}$$

$$\frac{d[C^+]_{in}}{dt} = j_{L,C^+} - j_P \tag{11}$$

where equations (4) and (7) in the main text give reaction rates $j_{L,x}$, j_P, respectively. Given that chemical species Y cannot cross the membrane, Y contributes to Q_{in} in time invariant manner determined by the initial conditions only. $k_{L,x}$, k_P in the equations (4) and (7) in the main text describe the detailed mechanism by which ions leak or are pumped across the biological membrane. In the main text we mentioned we chose k_P to be a constant and $k_{L,x}$ we base on Eyring's model [13] (equation (9) of the main text).

Choosing the forward rate of pumping k_P to be a constant implies the choice of a reversible rate function that describes at least a 2-step reaction operating always in the saturating regime for all its input variables (substrate/product concentrations and voltage), *i.e.* we assume $k_P \approx N_{Pump} \cdot v_{max}$ where N_{Pump} is the number of pumps and v_{max} the maximum rate per pump. In general, k_P is expected to depend on the input variables, and one can derive the specific functional dependency if one assumes a particular mechanism of action for the pump. To do so, we would also need to specify additional parameters characteristic for a given pump, such as affinities for its substrate, dependency on V_m, etc. This is out of the scope of this work, where we model a generic pump, and we refer the reader to [14] to find some examples of other rate laws for electrogenic pumps.

Eyring's model for $k_{L,x}$ is a special case of the so-called trapezoidal energy barrier model, which is a general model for describing the dynamics of ionic leakage across the membrane and is given as

$$j_{L,x} = \frac{S_{cell}}{V_{cell}} P_x \cdot b \cdot u \frac{[x]_{out} \cdot e^{u/2} - [x]_{in} \cdot e^{-u/2}}{e^{bu/2} - e^{-bu/2}} \tag{12}$$

where $u = -\frac{F}{RT} \cdot V_m$, P_x the so-called apparent permeability of the membrane for species x, and b is the so-called fractional width of the trapezoid. The SI Eq. (12) is the Eq. 7 in [13], which we multiply by $\frac{S_{cell}}{V_{cell}}$ to have the flux in units mole/volume/time rather than mole/surface/time, and which was first derived in [15, 16].

The apparent permeability is defined as: $P_x = \overline{P}_x \cdot \frac{[x]_{out}^{(interface)}}{[x]_{out}^{(bulk)}}$ where $\overline{P}_x$ is the specific permeability of the membrane for x and $[x]_{out}^{(interface)}$, $[x]_{out}^{(bulk)}$ are respectively the concentrations of x at the interface of the membrane and in the bulk (far away from the membrane). When $V_m = 0$ we expect $[x]_{out}^{(interface)} = [x]_{out}^{(bulk)}$ and the apparent and specific permeabilities to be identical. When $V_m \neq 0$ the ionic concentrations at the membrane is different compared to the bulk, ordinarily positive at the extracellular and negative at the intracellular interface, which can influence the *apparent* membrane permeability (see section 4 of [17] for more details).

In Eq. (12) b is parameter that characterizes the shape of the voltage drop across the membrane ($0 \leq b \leq 1$). More specifically, b characterizes $\frac{dV(z)}{dz}$ where z denote the position within the membrane. If $b = 0$, $V(z)$ abruptly changes in the middle of the lipid bilayer such that $\frac{dV(z)}{dz} = 0$ everywhere but at the geometrical middle of the membrane. This is known as the single Eyring barrier assumption and taking into the account the equation for the electrochemical potential (8) given in the main text, it reduces the SI Eq. (12) to:

$$j_{L,x} = \frac{S_{cell}}{V_{cell}} P_x \cdot [x]_{out} \cdot e^{-\frac{F}{2RT} \cdot z_x \cdot V_m} \cdot \left(1 - e^{\frac{\Delta G_x}{RT}}\right) \tag{13}$$

which is equivalent to the equations (7) and (9) in the main text. If $b = 1$, $\frac{dV(z)}{dz} = \text{constant}$ across the membrane. This was assumed by Goldman to derive the Goldman–Hodgkin–Katz (GHK) flux equation, and it it reduces the SI Eq. (12) to:

$$j_{L,x} = -\frac{S_{cell}}{V_{cell}} P_x \frac{z_x F}{RT} \cdot V_m \frac{[x]_{out}}{1 - e^{\frac{z_x F}{RT} V_m}} \cdot \left(1 - e^{\frac{\Delta G_x}{RT}}\right) \tag{14}$$

If $V_m < 0$, $\Delta G_x < 0$, $j_{L,x} > 0$ species x moves from the outside to the intracellular environment, as expected. As mentioned before, we use Eyring's assumption for our simulations and, for simplicity, we also assume that the surface partition coefficient $\frac{[x]_{out}^{(interface)}}{[x]_{out}^{(bulk)}}$ is constant, thus P_x is a constant as well.

Detailed derivation of SI equations (13) and (14) To obtain Eqs. (13) and (14) from Eq. (12) we first notice that $\Delta G_x/RT = -u + \ln([x]_{in}/[x]_{out})$ so that Eq. (12) becomes:

$$\begin{aligned} j_{L,x} &= \frac{S_{cell}}{V_{cell}} P_x \cdot b \cdot u \frac{[x]_{out} e^{u/2}}{e^{bu/2} - e^{-bu/2}} \left(1 - \frac{[x]_{in}}{[x]_{out}} e^{-u}\right) \\ &= \frac{S_{cell}}{V_{cell}} P_x \cdot b \cdot u \frac{[x]_{out} e^{u/2}}{e^{bu/2} - e^{-bu/2}} \left(1 - e^{\frac{\Delta G_x}{RT}}\right) \\ &= \frac{S_{cell}}{V_{cell}} P_x \cdot b \cdot u \frac{[x]_{out}}{e^{(b-1)u/2} - e^{-(b+1)u/2}} \left(1 - e^{\frac{\Delta G_x}{RT}}\right) \end{aligned} \tag{15}$$

When $b = 1$, Eq. (15) is equivalent to:

$$j_{L,x} = \frac{S_{cell}}{V_{cell}} P_x \cdot u \frac{[x]_{out}}{1 - e^{-u}} \left(1 - e^{\frac{\Delta G_x}{RT}}\right) \tag{16}$$

Which is equivalent to Eq. (8) in [13].

In order to show how to obtain Eq. (13) from Eq. (12) we first introduce the hyperbolic sinus: $2 \cdot \sinh(bu/2) = e^{bu/2} - e^{-bu/2}$ such that Eq. (15) is written:

$$j_{L,x} = \frac{S_{cell}}{V_{cell}} P_x \cdot b \cdot u \frac{[x]_{out} e^{u/2}}{2\sinh(bu/2)} \left(1 - e^{\frac{\Delta G_x}{RT}}\right) \tag{17}$$

We then use the fact that $\lim_{b \to 0} \left(\frac{2\sinh(bu/2)}{b}\right) = u$ and consequently when $b \to 0$ Eq. (17) reduces to Erying's rate equation (13).

Numerical simulations

The first step of our numerical experiment consists in finding parameter sets consistent with establishing a particular value of $V_{m,0}$, that is the membrane voltage in the absence of the dye. We assume that before the addition of the dye, the cell is in steady-state $\forall x : dx/dt = 0$ and consequently:

$$\frac{d[A^-]_{in}}{dt} = 0 \Leftrightarrow \Delta G_{L,A^-} = 0 \tag{18}$$

$$\frac{d[C^+]_{in}}{dt} = 0 \Leftrightarrow j_P = j_{L,C^+} \tag{19}$$

Thus, at steady-state, A^- equilibrates according to Nernst Eq. (2) in the main text and C^+ according to Eq. (11) in the main text. Consequently, to obtain the $V_{m,0}$ we solve the following ordinary differential equation system in a 3-dimensional grid $\{\Delta G_E, [Y]_{in}, \rho\}$ (see SI Table 4):

$$\frac{d[A^-]_{in}}{dt} = 1 - e^{\frac{\Delta G_{A^-}}{RT}} \tag{20}$$

$$\frac{d[C^+]_{in}}{dt} = 1 - e^{\frac{\Delta G_{C^+}}{RT}} - \rho \cdot \left(1 - e^{\frac{\Delta G_P}{RT}}\right) \tag{21}$$

As shown in Fig. SI1, the influence of the dye on ΔV_m depends on how $V_{m,0}$ was generated, and we can achieve the same value of $V_{m,0}$ by different parametrizations of $\{\rho, \Delta G_E, [Y]_{in}\}$.

The second part of the numerical experiment consists of choosing a starting steady-state set of values for $\{V_{m,0}, \Delta G_E, [Y]_{in}\}$ and a given $[Dye]_{out}$. We also select the values for the permeability of the membrane to cations, anions and the dye (P_{C^+}, P_{A^-} and P_{Dye}, respectively) and keep them fixed through out the experiment (values are given in SI Table 3). Lastly, to obtain the dye equilibration profile we need to implement the rate-laws for pumping and leakage we discussed above, and then solve the ODE system of SI equations (9) to (11) using the stiff solver "ode15s" from MATLAB R2018b. The initial *intracellular* concentration of the dye we chose is $[Dye]_{in} = 10^{-10} mM$, and the k_P value is chosen based on the steady-state solution for $V_{m,0}$ and using Eq. (10) in the main text. Specifically, for a chosen set of $\{V_{m,0}, \Delta G_E, [Y]_{in}\}$ we find ρ that gives $V'_{m,0} \approx V_{m,0}$ and use it to set k_P from the definition of ρ in Eq. (10) in the main text:

$$k_P = \frac{S_{cell}}{V_{cell}} \cdot P_{C^+} \cdot [C^+]_{out} \cdot \rho(V'_{m,0}) \cdot e^{-\frac{FV'_{m,0}}{2RT}}. \tag{22}$$

Distinguishing the inner from the outer membrane

In the main text we assumed cell's cytoplasm is separated from the environment by one membrane, effectively ignoring any potential charge separation across the outer membrane of *E. coli*. While active transport of cations proceeds across the inner membrane for the case of *E. coli*, e.g. NhaA [18] or KefB/C [19], surface charge on the outer membrane can lead to Donnan potential [20, 21], and we call this trans-outer-membrane voltage V_p. In the absence of pumps moving cations between the periplasmic and extracellular space, the ions equilibrate across the outer membrane according to Nernst equation. Therefore, for the periplasmic concentrations we can write:

$$[C^+]_p = [C^+]_{out} \cdot e^{-\frac{F}{RT}V_p} \tag{23}$$

$$[Dye^+]_p = [Dye^+]_{out} \cdot e^{-\frac{F}{RT}V_p} \tag{24}$$

$$[A^-]_p = [A^-]_{out} \cdot e^{+\frac{F}{RT}V_p} \tag{25}$$

We used the measured value for $V_p \sim -30$ mV (negative in the periplasm) [21] to estimate $[Dye^+]_p \approx 3.2 \times [Dye^+]_{out}$. Thus, in the presence of such a V_p, the overall membrane voltage $V_m^\star$ would become $V_m^\star = V_m + V_p$ [11] and the impact of the dye on V_m is as if there was no V_p but the $[Dye_{out}]$ was ~ 3.2 times greater. Similarly, to account for the effect of the trans-outer-membrane voltage, all the concentrations $[x]_{out}$ refered to in the main text should be corrected by a factor $e^{-z_x \frac{F}{RT}V_p}$.

REFERENCES

[1] N. Lord, *Fluctuation timescales in bacterial gene expression*. PhD thesis, Harvard University, 2014.

[2] T. Pilizota and J. W. Shaevitz, "Fast, multiphase volume adaptation to hyperosmotic shock by escherichia coli," *PLOS ONE*, vol. 7, pp. 1–10, 04 2012.

[3] E. Krasnopeeva, C.-J. Lo, and T. Pilizota, "Single-cell bacterial electrophysiology reveals mechanisms of stress-induced damage," *Biophysical Journal*, vol. 116, no. 12, pp. 2390 – 2399, 2019.

[4] Y. Wang, E. Krasnopeeva, S. Lin, F. Bai, T. Pilizota, and C. Lo, "Comparison of escherichia coli surface attachment methods for single-cell, in vivo microscopy," *In preparation*, 2019.

[5] M. Basan, M. Zhu, X. Dai, M. Warren, D. Sévin, Y.-P. Wang, and T. Hwa, "Inflating bacterial cells by increased protein synthesis," *Molecular Systems Biology*, vol. 11, no. 10, 2015.

[6] W. Bai, K. Zhao, and K. Asami, "Dielectric properties of e. coli cell as simulated by the three-shell spheroidal model," *Biophysical Chemistry*, vol. 122, no. 2, pp. 136 – 142, 2006.

[7] P. F. Costa, M. G. Emilio, P. L. Fernandes, H. G. Ferreira, and K. G. Ferreira, "Determination of ionic permeability coefficients of the plasma membrane of xenopus laevis oocytes under voltage clamp.," *The Journal of Physiology*, vol. 413, no. 1, pp. 199–211, 1989.

[8] J. Rosko, V. A. Martinez, W. C. K. Poon, and T. Pilizota, "Osmotaxis in escherichia coli through changes in motor speed," *Proceedings of the National Academy of Sciences*, 2017.

[9] K. A. Martinez, R. D. Kitko, J. P. Mershon, H. E. Adcox, K. A. Malek, M. B. Berkmen, and J. L. Slonczewski, "Cytoplasmic ph response to acid stress in individual cells of escherichia coli and bacillus subtilis observed by fluorescence ratio imaging microscopy," *Applied and Environmental Microbiology*, vol. 78, no. 10, pp. 3706–3714, 2012.

[10] E. Krasnopeeva, *Single cell measurements of bacterial physiology traits during exposure to an external stress*. PhD thesis, University of Edinburgh, 2018.

[11] M. Grabe and G. Oster, "Regulation of organelle acidity," *The Journal of General Physiology*, vol. 117, no. 4, pp. 329–344, 2001.

[12] R. Buda, Y. Liu, J. Yang, S. Hegde, K. Stevenson, F. Bai, and T. Pilizota, "Dynamics of escherichia coli's passive response to a sudden decrease in external osmolarity," *Proceedings of the National Academy of Sciences*, vol. 113, no. 40, pp. E5838–E5846, 2016.

[13] K. D. Garlid, A. D. Beavis, and S. K. Ratkje, "On the nature of ion leaks in energy-transducing membranes," *Biochimica et Biophysica Acta (BBA) - Bioenergetics*, vol. 976, no. 2, pp. 109 – 120, 1989.

[14] J. Keener and J. Sneyd, *Mathematical Physiology*, p. 93. 2009.

[15] J. E. Hall, C. A. Mead, and G. Szabo, "A barrier model for current flow in lipid bilayer membranes," *The Journal of Membrane Biology*, vol. 11, pp. 75–97, Dec 1973.

[16] W. Morf, *The Principles of Ion-selective Electrodes and of Membrane Transport*. Studies in analytical chemistry, New York, 1981.

[17] H. Butt, M. Karlheinz Graf, H. Butt, K. Graf, and M. Kappl, *Physics and Chemistry of Interfaces*. Physics textbook, Wiley, 2003.

[18] I. T. Arkin, H. Xu, M. Ø. Jensen, E. Arbely, E. R. Bennett, K. J. Bowers, E. Chow, R. O. Dror, M. P. Eastwood, R. Flitman-Tene, B. A. Gregersen, J. L. Klepeis, I. Kolossváry, Y. Shan, and D. E. Shaw, "Mechanism of na+/h+ antiporting," *Science*, vol. 317, no. 5839, pp. 799–803, 2007.

[19] M. Papanastasiou, G. Orfanoudaki, M. Koukaki, N. Kountourakis, M. F. Sardis, M. Aivaliotis, S. Karamanou, and A. Economou, "The escherichia coli peripheral inner membrane proteome," *Molecular & Cellular Proteomics*, vol. 12, no. 3, pp. 599–610, 2013.

[20] P. Nelson, *Biological Physics (Updated Edition)*. 2003.

[21] J. B. Stock, B. Rauch, and S. Roseman, "Periplasmic space in salmonella typhimurium and escherichia coli.," *Journal of Biological Chemistry*, vol. 252, no. 21, pp. 7850–61, 1977.